Received: 31 March 2020 | Accepted: 10 August 2020

DOI: 10.1002/maco.202011707

ARTICLE

Materials and Corrosion

The kinetics of copper corrosion in nitric acid

Joseph Turnbull[1] | **Ryan Szukalo**[1] | **Dmitrij Zagidulin**[1] | **Mark Biesinger**[2] | **David Shoesmith**[1,2]

[1]Department of Chemistry, University of Western Ontario, London, Ontario, Canada

[2]Surface Science Western, University of Western Ontario, London, Ontario, Canada

Correspondence
David Shoesmith, Department of Chemistry, University of Western Ontario, 1151 Richmond St., London, ON N6A 5B7, Canada.
Email: dwshoesm@uwo.ca

Funding information
NSERC Discovery Grant; Nuclear Waste Management Organization

Abstract

The strategy for the permanent disposal of high-level nuclear waste in Canada involves sealing it in a copper-coated steel container and burying it in a deep geologic repository. During the early emplacement period, the container could be exposed to warm humid air, which could result in the condensation of nitric acid, produced by the radiolysis of the humid air, on the copper surface. Previous studies have suggested that both nitrate and oxygen reduction will drive copper corrosion, with the nitrate reduction kinetics being dependent on the concentration of soluble copper(I) produced by the anodic dissolution of copper in the reaction with oxygen. This study focused on determining the kinetics of nitrate and oxygen reduction and elucidating the synergistic relationship between the two processes. This was investigated using corrosion potential and polarization measurements in conjunction with scanning electron microscopy and X-ray photoelectron spectroscopy. Oxygen reduction was shown to be the dominant cathodic reaction with the oxidation of copper(I) to copper(II) by nitrate, promoting the catalytic cycle involving the reaction of copper(II) with copper to reproduce copper(I).

KEYWORDS

copper, corrosion, electrochemistry, kinetics, nitric acid, nuclear waste disposal

1 | INTRODUCTION

For nuclear power to remain a viable energy source, the safe management of high-level nuclear waste is necessary. The international approach to its disposal is to seal the waste in corrosion-resistant containers and bury it in a deep geologic repository (DGR). In Canada, the proposed container consists of a carbon steel vessel coated with approximately 3 mm of copper applied via electrodeposition and cold spray technologies. The DGR concept and container design have been described in detail elsewhere.[1–6]

An essential requirement in the performance assessment of the proposed copper-coated steel container is a comprehensive model to simulate the reactions and interactions that will occur over the lifetime of the container. When developing such a model, the kinetic information for each corrosion process must be well understood to ensure a meaningful simulation. Current models outline many of the major corrosion processes.[7–11] However, a model that assesses the influence of radiolysis on the corrosion of the copper coating does not yet exist.[6] As humid air radiolysis is a short-term process that could cause some corrosion damage without leading to container failure,[12–14] it may be sufficient to determine the nature and extent of corrosion damage, leading to the specification of a corrosion allowance for this process. To achieve this, a thorough understanding of the mechanism of the corrosion process is required.

Many reactive species can result from the gamma radiolysis of humid air, with one of the most important

species being nitric acid.[12–14] The influence of radiation on copper corrosion in humid air has been studied and discussed.[15] More recent studies have shown that whereas minimal corrosion was observed at the low gamma radiation dose rates anticipated in a DGR,[16] substantial corrosion occurred at much higher dose rates.[17] Radiolysis model calculations show that significant amounts of nitric acid could be produced at dose rates relevant to DGR conditions.[14]

In a previous work,[15] the corrosion process in both aerated and deaerated nitric acid solutions was investigated by following the pH and the concentration of dissolved copper in a small volume of the solution designed to simulate the limited amounts of water that will condense on the container surface. These studies showed that negligible corrosion occurred in anoxic nitric acid, but the corrosion rate increased markedly when oxygen was added. On the basis of pH measurements, it appeared that the nitric acid became activated as a cathodic reagent when oxygen was present.[15] It was proposed that this could be attributed to the catalytic influence of copper(I).[15,18,19] As the experiments were conducted in a small solution volume, saturation of the solution with dissolved copper(I)/copper(II) led to the deposition of a substantial layer of corrosion products and the apparent suppression of the overall corrosion process. As both possible cathodic reactions consumed H^+, reactions (1) and (2):

$$NO_3^- + 2H^+ + 2e^- \rightarrow H_2O + NO_2^-, \quad (1)$$

$$\frac{1}{2}O_2 + 2H^+ + 2e^- \rightarrow H_2O. \quad (2)$$

The evolution of pH with time provided a means of following the kinetics of the corrosion process, but could not differentiate the relative importance of the two reactions.[15]

In this study, the corrosion mechanism is investigated using electrochemical and surface analytical measurements, with the primary goal of determining which of the two cathodic reagents is dominant and whether the cathodic reaction involving nitrate is catalyzed by the presence of copper(I). To avoid the complications resulting from the deposition of corrosion products, experiments were conducted in the presence of a large solution volume, that is, experiments were conducted in a cell with a very small electrode surface area-to-solution volume ratio.

2 | EXPERIMENTAL

All electrodes for electrochemical experiments were $1 \times 1 \times 1$-cm cubes of oxygen-free, phosphorous-doped copper, supplied by Svensk Kärnbränslehantering AB, Solna, Sweden. The cubes were attached to a steel dowel by a threaded hole. All but one surface of the copper coupon were isolated from the solution using Epofix epoxy and the steel dowel was isolated using polytetrafluoroethylene shrink tubing. The exposed copper surface was subsequently prepared using a series of silicon carbide grinding pads ranging between P800 and P2400. After grinding, the sample was placed in an ultrasonic bath with methanol for 2 min, followed by water for an additional minute before being dried in an argon stream. For experiments performed under anoxic conditions, a final polishing step to achieve the final surface finish was performed inside an anaerobic chamber.

Solutions were prepared by mixing the appropriate volumes of nitric acid, provided by Caledon, and Type-1 water with a resistivity of 18.2 MΩ·cm, collected from a Barnstead Nanopure water purification system provided by Thermo Fisher Scientific. Sodium nitrate, provided by Caledon, was added to solutions when necessary. Aerated solutions were left open to the atmosphere to allow gas exchange between the headspace of the electrochemical cell and the surrounding atmosphere. Experiments conducted using specific oxygen concentrations were constantly sparged at 0.1 L/min using various ratios of pure oxygen and argon. The flow rate and the ratios of the two gases were achieved using two gas mass flow controllers provided by Alicat Scientific and controlled by in-house designed software. Solutions were sparged for 20 min before the start of an experiment to ensure that equilibrium between the gas and solution had been achieved. Conversions from oxygen vol% to concentration were done using Henry's Law:

$$H^{cp} = \frac{c_{O_2}}{\rho}, \quad (3)$$

where H^{cp} is Henry's constant (1.3×10^{-3} mol·L^{-1}·atm^{-1}[20]), c_{O_2} is the aqueous concentration of oxygen, and ρ is the oxygen partial pressure. Anoxic experiments were performed in an Innovative Technology PureLab HE argon-filled glovebox equipped with an oxygen sensor to ensure that the oxygen concentration remained below 0.1 ppm in the chamber.

Electrochemical experiments were performed in a standard, three-electrode glass cell. A solution volume of 500 mL was used to achieve an electrode surface area-to-volume (SA/V) ratio of 0.002 cm^{-1} and to avoid exceeding solubility limits for copper oxides/hydroxides. A piece of platinum foil attached to a platinum wire acted as the counter electrode, and potentials were measured against a saturated calomel electrode (SCE; 0.241 V vs. standard hydrogen electrode).[21] All electrochemical measurements were conducted inside a grounded Faraday cage to minimize interferences from

external electrical fields. A Solartron 1480 MultiStat was used to control applied potentials and record current responses. CorrWare (v. 3.4d) software (Scribner Associates) was used to control instrumentation and to record and analyze data. Corrosion potential (E_{corr}) measurements were collected for various periods of time, followed by polarization resistance (R_p) measurements, using the linear polarization resistance technique, conducted at a scan rate of 0.167 mV/s with vertices ~5 mV versus E_{corr}. All samples underwent cathodic cleaning before each experiment using a two-step potentiostatic sequence, 1 min held at −1.5 V versus SCE and then 1 min held at −1.15 V versus SCE.

Scanning electron microscopy (SEM) images were collected using a Hitachi SU3500 Variable-Pressure SEM. The electron beam was accelerated between 15 and 25 kV at a working distance of 10 mm and rastered across the sample surface to collect high-resolution images. X-ray photoelectron spectroscopic (XPS) analyses were performed using a Kratos AXIS Ultra Spectrometer with a monochromatic Al K_α (15 mA, 14 kV) radiation source ($h\upsilon = 1{,}486.6$ eV). The instrument work function was calibrated against the Au $4f_{7/2}$ metallic gold binding energy, 83.95 eV, and when necessary, the carbon–carbon peak of the carbon 1s spectrum was set to 284.8 eV to correct for charging. Survey spectra were collected over the binding energy range 0–1,100 eV. High-resolution spectra were recorded for copper $2p_{3/2}$ (929.5–953.5 eV), oxygen 1s (527.5–543.5 eV), carbon 1s (281.5–298.5 eV), and the Auger copper LMM peak (563.5–583.5 eV). All spectra were subsequently analyzed using CasaXPS software and peak-fitting procedures as described elsewhere.[22] The procedure used to avoid air exposure while transferring specimens to the spectrometer has been described elsewhere.[23]

3 | RESULTS AND DISCUSSION

3.1 | The influence of nitrate and pH

Measurements of E_{corr} and R_p were performed over a 14-day period in various aerated nitric acid solutions ranging in concentration from 10 to 150 mM (Figure 1). Despite the change in the nitric acid concentration, neither E_{corr} nor R_p changed significantly (after an initial period of ~0.5 days), suggesting that neither nitrate concentration nor H^+ concentration affected the corrosion rate. The initial slight change in E_{corr} was most likely due to the re-establishment of the open circuit condition after the cathodic cleaning process, which would involve processes such as the relaxation of adsorbed surface states and the transport-controlled readjustment of the local pH. After ~1 day, E_{corr} stabilized and increased only very slightly (~1 mV) for the remainder

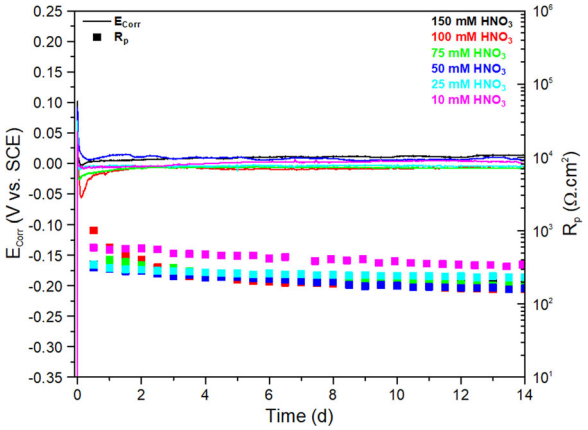

FIGURE 1 E_{corr} and R_p measurements in aerated HNO_3 solutions. SCE, saturated calomel electrode [Color figure can be viewed at wileyonlinelibrary.com]

of the experiment. By contrast, R_p exhibited a slow decrease beyond the initial stabilization period. This suggested that the rate of the cathodic reaction increased slightly over the entire experiment. The short-term changes in E_{corr} and R_p most likely reflect the roughening of the copper surface, resulting in a slightly increased surface area to support the cathodic reaction. The slow increase in the rate over the period of 2–14 days could have reflected a slow increase in the rate due to the activation of nitrate reduction attributable to the slow accumulation of dissolved copper(I) species.[15,18,19]

To confirm that neither nitrate concentration nor H^+ concentration affected the corrosion rate under aerated conditions, a second set of experiments was carried out, where the nitrate concentration was kept constant at 150 mM, whereas the H^+ concentration was changed (Figure 2). A comparison between the two data sets showed no significant difference, confirming that the overall corrosion rate was of zero order with respect to both nitrate concentration and H^+ concentration.

3.2 | The influence of oxygen

E_{corr} and R_p values were measured on a copper electrode immersed in either aerated, argon-sparged, or anoxic solutions containing 100-mM nitric acid, Figure 3. The initial E_{corr} values in the solutions were very similar, ~70 mV (vs. SCE), but they decreased rapidly to approximately −40 mV (vs. SCE). As observed in Figure 1, in the aerated solution, E_{corr} increased only slightly over the 7-day exposure period, accompanied by a slight decrease in R_p (increase in the corrosion rate). In the argon-sparged solution, when only a residual oxygen concentration would have been present (~10^{-6} M), E_{corr}

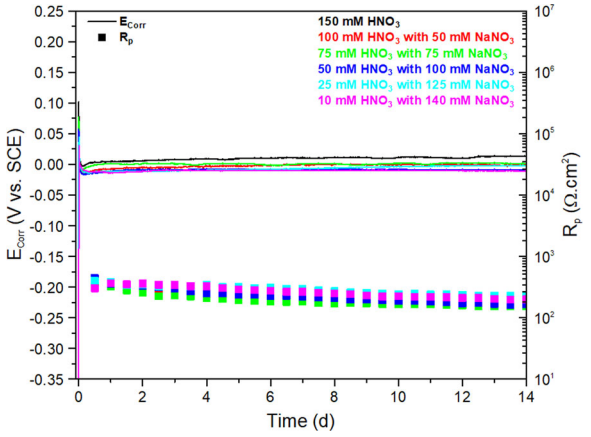

FIGURE 2 E_{corr} and R_p measurements in aerated HNO_3 solutions with constant $[NO_3^-] = 150$ mM. SCE, saturated calomel electrode [Color figure can be viewed at wileyonlinelibrary.com]

decreased to an approximate steady-state value after 1 day, during which positive-going E_{corr} transients were observed. During the same time, R_p increased to an approximate steady-state value ~10^2 times greater than that achieved under aerated conditions, confirming a major drop in the corrosion rate when the availability of oxygen was limited. In anoxic solutions, when the oxygen concentration would be ~10^{-9} M,[24] E_{corr} was approximately the same as in the aerated solution, before decreasing slowly to a value less than that observed in argon-sparged conditions. This decrease was accompanied by an increase in R_p to a value ~3 times than that observed under argon-sparged conditions. This measurable difference in the long-term R_p values between argon-sparged and anoxic conditions indicated that the corrosion process was very sensitive to small oxygen concentrations. As observed in argon-sparged conditions, a series of positive-going E_{corr} transients was observed over the first 2.5–3 days of exposure.

Unlike the other two specimens, the electrode used in the anoxic experiment inside the glovebox was not subjected to cathodic cleaning. Consequently, the observed decrease in E_{corr} can be attributed to the chemical dissolution of an air-formed oxide present at the start of the experiment. Irrespective of these uncertainties in the short-term behavior, the long-term increase in R_p, accompanied by a low E_{corr} value, confirmed that the corrosion rate was extremely low in the absence of oxygen.

Sections of the E_{corr} curves recorded between 1.1 and 1.4 days are shown in Figure 4. Whereas no potential transients were observed in aerated conditions when the corrosion rate was high, metastable pitting transients were observed at the two low oxygen concentrations, with the frequency and amplitude most marked under argon-sparged conditions. Although the trends did not correlate directly with oxygen concentrations, these transients suggested that when small to negligible oxygen concentrations were present, the copper surface tended to passivate, as noted previously.[15] The disappearance of transients (beyond 2.5–3.0 days) suggests a passivating role for nitrate, either by chemisorption or oxide formation, as previously suggested.[15] It is likely that at low oxygen concentrations, these transients reflect a competition between the passivating influence of nitrate and the activating influence of oxygen. The numerous transients observed when small oxygen concentrations were present (argon-sparged conditions) could then be attributed to

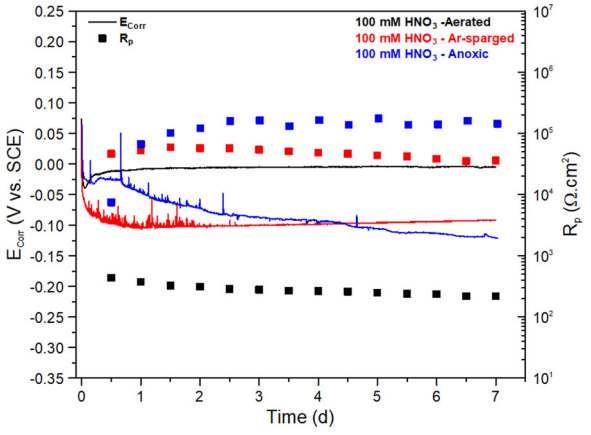

FIGURE 3 E_{corr} and R_p measurements in 100-mM HNO_3 solutions under aerated, Ar-sparged, and anoxic conditions. SCE, saturated calomel electrode [Color figure can be viewed at wileyonlinelibrary.com]

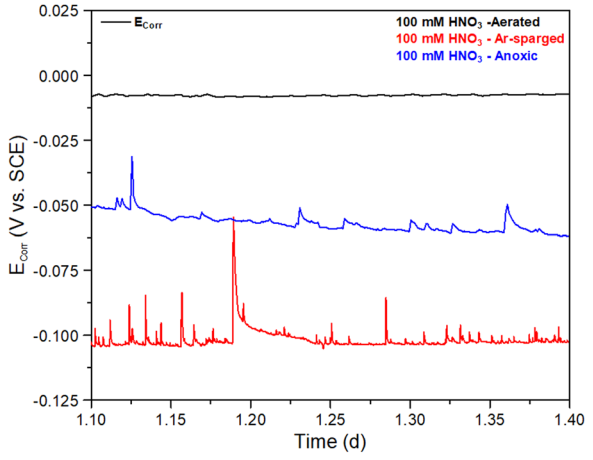

FIGURE 4 E_{corr} and R_p measurements for the time period of 1.1–1.4 days in 100-mM HNO_3 solutions under aerated, Ar-sparged, and anoxic conditions. SCE, saturated calomel electrode [Color figure can be viewed at wileyonlinelibrary.com]

temporary support of corrosion at film breakdown sites by oxygen reduction. This would initially have stimulated localized corrosion, but the rapid local depletion of oxygen would subsequently have allowed nitrate to repassivate the breakdown site. The decreased transient frequency under anoxic conditions could have been related to the air-formed oxide present on this electrode and its subsequent dissolution, or to the decreased oxygen concentration, resulting in fewer film breakdown events. However, currently available data could not determine the relative contributions of these influences.

SEM images of the electrode surface after 7 days of exposure in aerated nitric acid, Figure 5a,b, demonstrated extensive crystallographic etching, whose extent depends on the grain orientation. The absence of any original polishing lines confirms the occurrence of active corrosion, as indicated by the low R_p values and the absence of transients in E_{corr} (Figure 3). Figure 5c,d shows SEM images of the surface after 7 days of exposure to argon-sparged nitric acid. As expected, considering the large R_p values (Figure 3), only minor corrosion occurred, as the original polishing lines remained clearly visible. The corrosion damage was located in a high density of small pits, consistent with the frequent occurrence of metastable film breakdown events. A closer examination of the dark patches visible in Figure 5c showed that these areas were not observably more corroded than other areas of the surface; however, increased carbon was detected by energy-dispersive X-ray spectroscopy.

SEM micrographs of the corroded surface after exposure under anoxic conditions, Figure 5e,f, exhibited a patchy deposit on the electrode surface. Some of the original grinding lines could still be observed; however, they are significantly less pronounced in comparison to the argon-sparged case. Considering the lack of cathodic cleaning and the constantly decreasing E_{corr} observed for this sample in Figure 3, this deposit was most likely a restructured oxide resulting from the chemical dissolution of tenorite (CuO) as copper(II), which could have subsequently reacted with copper to produce cuprite (Cu_2O). Thus, this morphology may not accurately represent the damage to a clean surface. The large, but infrequent, crystals present on this surface were sodium chloride crystals deposited during the incomplete washing and drying of the electrode before transfer to the microscope.

These results clearly demonstrated that when oxygen was present, blockage of the copper surface by either

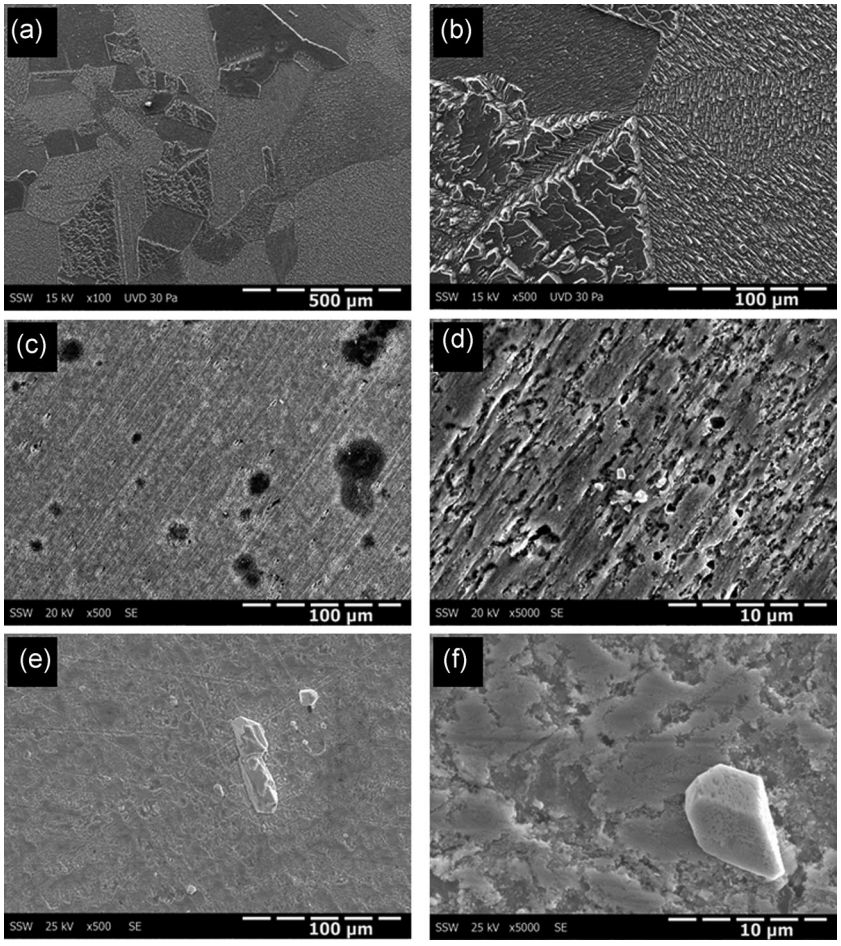

FIGURE 5 Scanning electron micrographs of Cu coupons after immersion in 100-mM HNO_3 for 7 days under (a,b) aerated, (c,d) Ar-sparged, and (e,f) anoxic atmospheres

chemisorbed nitrate or oxide formation due to oxidation by nitrate did not occur. In aerated nitric acid, when the oxygen concentration was high, copper could be rapidly dissolved as copper(II).[25,26] In argon-sparged and anoxic conditions, corrosion was inhibited despite the ability of nitrate to act as an oxidant, consistent with literature claims that nitrate reduction was blocked on Cu surfaces.[18,25] A number of studies have shown that, depending on the copper crystal plane, nitrate reduction was either completely blocked or proceeded very slowly.[27,28] Based on in-situ electrochemical scanning tunneling microscopy and enhanced Raman spectroscopy studies, this was attributed to either the chemisorption of nitrate or to the formation of cuprite by the extraction of an oxygen atom from adsorbed nitrate.[27] The formation of these potentially passivating layers was consistent with the observation of E_{corr} transients, indicating metastable breakdown events on a generally unreactive surface. The positive-going nature of these transients would be consistent with a sudden increase in the rate of the cathodic reaction at a local breakdown site, followed rapidly by repair of the location by either the readsorption of nitrate or the reformation of cuprite.

XPS analyses of the corroded samples exposed to aerated and argon-sparged 100-mM nitric acid were performed. Each spectrum was fitted and analyzed using the methods developed by Biesinger et al.[20,29,30] Based on the survey spectra, the two samples exhibited significantly different surface compositions, with the most notable difference being the presence of nitrogen on the sample exposed under argon-sparged conditions (Table 1). Copper $2p_{3/2}$ and copper LMM high-resolution spectra were used to determine the chemical states of copper on the electrode surfaces. The electrode corroded under aerated conditions exhibited a film primarily composed of copper(0) and copper(I) species (Figure 6). The copper $2p_{3/2}$ spectrum, Figure 6a, was analyzed based on the calculations outlined by Biesinger et al.[22] to determine the ratios of copper(0) and copper(I) to copper(II) based on the areas of peaks (A) and (B) with intensity reported in counts per second. This calculation considered that the main emission line (A) contained contributions from both copper oxidation states, copper(I)/copper(II), but the intensity of the shake-up satellite peak (B) contained a contribution from copper(II) only. This analysis showed that the majority of copper on the surface is in either the copper(0) or copper(I) state, with copper(II) present in only minor amounts (~14%).

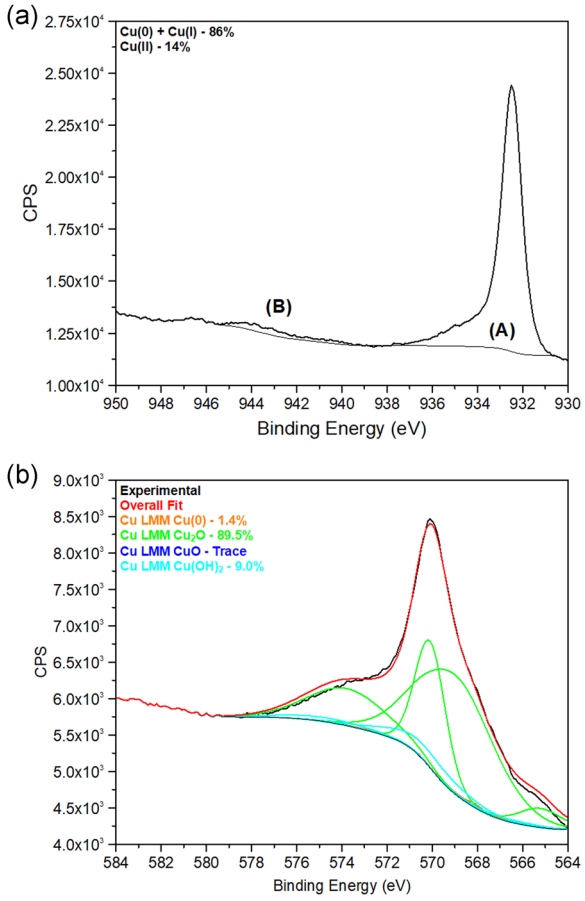

FIGURE 6 (a) Cu $2p_{3/2}$ and (b) Cu LMM high-resolution spectra recorded on a Cu specimen immersed in aerated 100-mM HNO_3 for 7 days [Color figure can be viewed at wileyonlinelibrary.com]

TABLE 1 Electrode surface coverage after corrosion in aerated and Ar-sparged 100-mM HNO_3, as determined by XPS

Element/transition	Aerated (at%)	Ar-sparged (at%)
Cu 2p 3/2	7.5	4.9
O 1s	25.8	22.8
N 1s	N/A	1.7
C 1s	57.7	65.3
Si 2s	8.7	4.7

Note: Traces of Hg and Pd from the reference and counter electrodes were also detected.
Abbreviation: XPS, X-ray photoelectron spectroscopy.

This was confirmed by curve fitting of the copper LMM spectrum, Figure 6b, which indicated that cuprite dominated the surface, ~89.5%, whereas copper(II) was present as a hydroxide, $Cu(OH)_2$, ~9%. The presence of cuprite can necessarily not be related to the corrosion process, as cuprite is a common air-formed oxide.[31] The electrode corroded under argon-sparged conditions demonstrated a more even distribution of each copper oxidation state (Figure 7). The copper $2p_{3/2}$ spectrum showed that copper(II) species were present in significant amounts, ~40%, in contrast to the ~14% observed in the

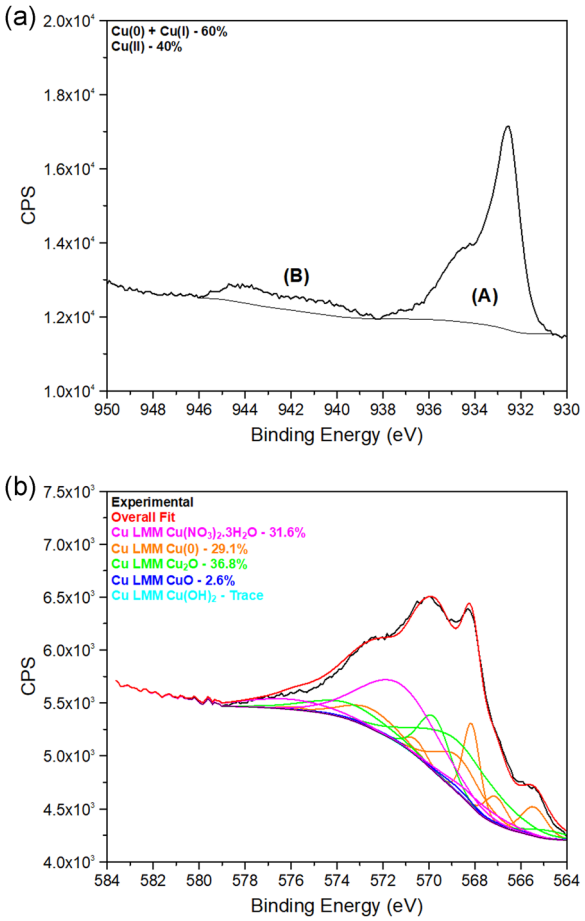

FIGURE 7 (a) Cu $2p_{3/2}$ and (b) Cu LMM high-resolution spectra recorded on a Cu specimen immersed in Ar-sparged 100-mM HNO_3 for 7 days [Color figure can be viewed at wileyonlinelibrary.com]

aerated case. The copper LMM analysis supported this, indicating that the majority of the copper(II) species were associated with nitrate, with only minor amounts of tenorite and $Cu(OH)_2$. The reported atomic percentages from the copper LMM spectra may be only approximate, as the fit assumed the presence of $Cu(NO_3)_2{\cdot}H_2O$ while multiple copper nitrates may be formed,[22] including rouaite ($Cu_2NO_3(OH)_3$), as reported in our previous study.[15]

While not definitive, these differences in the surface composition were instructive when determining the different processes occurring under the two conditions. Under aerated conditions, the electrochemical and SEM analysis demonstrated that rapid dissolution occurred. However, copper(II) species were relatively sparse on the electrode surface and only present as small amounts of $Cu(OH)_2$. Under acidic conditions, these hydroxide species should be very soluble, allowing for continuous active corrosion, as seen in previous studies.[31] In the argon-sparged experiment, when only traces of oxygen were present, the small amounts of copper(I) formed appeared to be rapidly oxidized by nitrate and collected on the copper surface as copper(II) nitrate solids. This observation supported claims made by Bae et al.[27] that the adsorption of nitrate on a copper surface was capable of oxidizing the surface while simultaneously blocking it. These observations support previous claims that nitrate reduction would freely occur in the presence of oxygen when copper(I) could be formed but would not react by itself.[18–20]

The influence of copper(I) on the activation of nitrate as an oxidant was investigated in experiments in which the solution was switched in mid-experiment between argon-sparging and aerated, and vice versa, Figures 8a and 8b, respectively. When the sample was initially exposed to an argon-sparged environment, Figure 8a, the behavior observed before adding oxygen closely reproduced the results plotted in Figure 3, with E_{corr} achieving a steady-state value of ~0.10 V with an R_p value

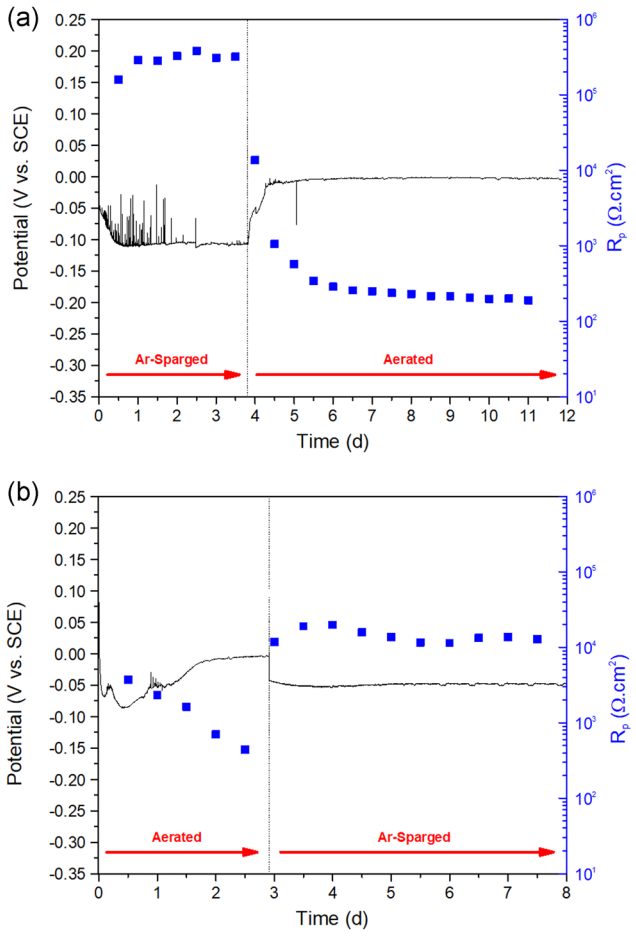

FIGURE 8 E_{corr} and R_p measurements recorded during the transition from (a) an Ar-sparged to aerated environment and (b) aerated to Ar-sparged environment in 100-mM HNO_3. SCE, saturated calomel electrode [Color figure can be viewed at wileyonlinelibrary.com]

$>10^5\ \Omega{\cdot}cm^2$. This steady-state R_p value was approximately one order of magnitude greater than that plotted in Figure 3, which could reflect both the sensitivity of R_p to low oxygen concentrations and the variability of the sparging process. As observed before, a series of E_{corr} transients, which disappeared after ~2 days, was observed. This was consistent with the instability of the surface due to competition between nitrate, which promoted passivity, and corrosion due to the action of trace oxygen.

When argon-sparging was stopped and atmospheric oxygen diffused into the solution, E_{corr} increased to a steady-state value of ~0 V, accompanied by a marked decrease in R_p to ~200 $\Omega{\cdot}cm^2$, consistent with the values observed in the experiment shown in Figure 3. The transition between steady-state values required >1 day, due to the combined effects of slow diffusion of oxygen into the solution and the gradual removal or dissolution of an inhibiting oxide or copper-nitrate formed under argon-sparged conditions. The chemical and oxidative dissolution of the species identified on the copper surface using XPS would proceed via the following reactions[31,32]:

$$CuO + 2H^+ \rightarrow Cu^{2+} + H_2O, \quad (4)$$

$$2Cu_2O + O_2 + 8H^+ \rightarrow 4Cu^{2+} + 4H_2O, \quad (5)$$

$$Cu_2NO_3(OH)_3 \rightarrow 2Cu^{2+} + NO_3^- + 3OH^-. \quad (6)$$

When copper was initially exposed to aerated conditions and then switched to argon-sparging, Figure 8b, the changes in E_{corr} and R_p were considerably less marked. The aerated E_{corr} increased and R_p decreased over the full 3-day exposure period. This indicated that the decrease in R_p and increase in E_{corr} could be attributed to an acceleration in the cathodic kinetics, despite the constant oxygen concentration over the exposure period. This would be consistent with a catalytic influence of copper(I) in activating nitrate as an oxidant, as proposed previously.[15,18,19] This claim was further supported by the behavior observed after subsequently switching to argon-sparged conditions. The low E_{corr} and very high R_p values shown for argon-sparged conditions in Figure 3 were not reproduced in this case. E_{corr} decreased to only −0.05 V and R_p increased to only ~10^4 $\Omega{\cdot}cm^2$ in contrast to the −0.10 V and $2 \times 10^5\ \Omega{\cdot}cm^2$, as previously observed. Thus, the enhanced corrosion rate established under aerated conditions was sustained, despite the removal of oxygen. This would be consistent with our claim that nitrate was activated as a cathodic reagent by the presence of copper(I), with corrosion proceeding via the reaction sequence:

$$NO_3^- + 2H^+ + 2e^- \rightarrow NO_2^- + 2H_2O, \quad (7)$$

$$2Cu^+ \rightarrow 2Cu^{2+} + 2e^-, \quad (8)$$

with copper(II) subsequently reacting with exposed copper

$$2Cu^{2+} + 2Cu \rightarrow 4Cu^+ \quad (9)$$

to yield the overall reaction[18,25]

$$NO_3^- + 2H^+ + 2Cu \rightarrow NO_2^- + H_2O + 2Cu^+. \quad (10)$$

Given the small SA/V ratio used in these experiments, the copper surface was blocked by corrosion products and remained available to maintain this reaction. This was in contrast to the previous study on a small solution volume when the deposition of corrosion products was observed to suppress the corrosion process.[15]

3.3 | Oxygen reduction reaction

Figure 9 shows the evolution of E_{corr} with time for the 11 tested oxygen/argon mixtures. As all electrodes were cathodically cleaned before the experiment, the influence of any air-formed oxide was likely to be short term and negligible beyond a few hours. Except for the electrode exposed to an argon-sparged solution (0% oxygen sparged), which reproduced the behavior shown for similar exposure conditions (Figure 3), E_{corr} increased for all oxygen concentrations, eventually achieving, or at lower oxygen concentrations approaching, a steady-state value. These changes were accompanied by decreases in R_p as the oxygen concentration was increased (Figure 10). This combination of increased E_{corr} values, accompanied by increased corrosion rates ($\propto R_p^{-1}$), when compared with the minimal changes in these parameters with [NO_3^-],

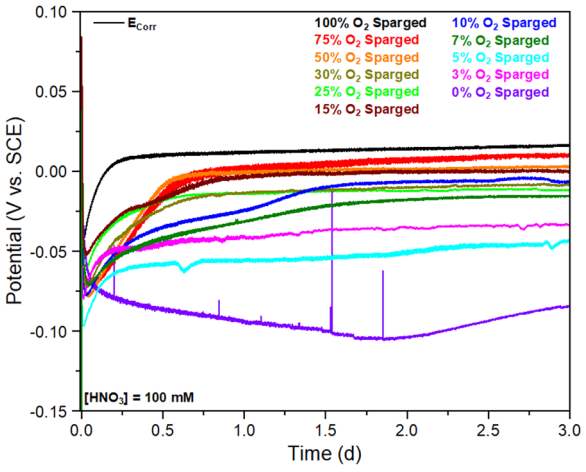

FIGURE 9 E_{corr} measurements for 100-mM HNO_3 solutions sparged with various O_2 percentages by volume. SCE, saturated calomel electrode [Color figure can be viewed at wileyonlinelibrary.com]

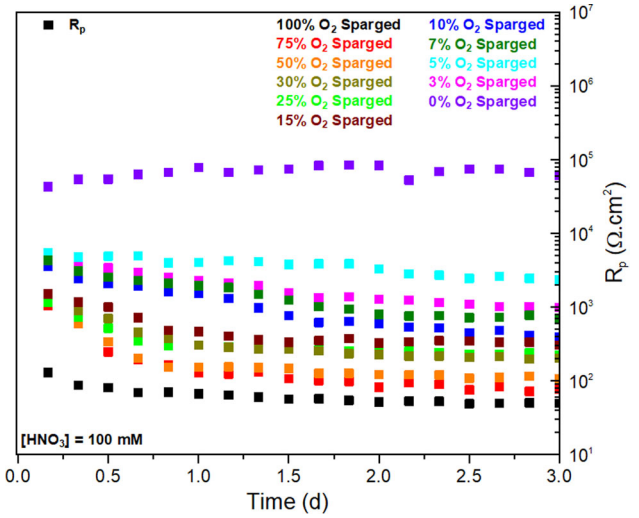

FIGURE 10 R_p measurements for 100-mM HNO_3 solutions sparged with various O_2 percentages by volume [Color figure can be viewed at wileyonlinelibrary.com]

confirmed that the kinetics of the oxygen reduction reaction was the dominant influence on the overall corrosion kinetics. As observed in Figures 9 and 10, R_p decreased as E_{corr} increased over the exposure period up to 1.5 days, with the change in R_p being directly related to the change in E_{corr}, as demonstrated in Figure 11 for the 10% oxygen case. Although not shown, similar linear relationships were observed for all oxygen concentrations. In general, the early changes in E_{corr} and R_p were accelerated as the oxygen concentration increased.

Two possible explanations exist for this acceleration: (a) the catalytic activation of the nitrate reduction reaction (discussed above), which would have accelerated as the surface concentration of copper(I) increased with the increasing oxygen concentration, or (b) catalysis of the oxygen reduction reaction itself by the formation of donor–acceptor (copper/copper(I)) sites on the copper surface, as demonstrated to occur under more neutral conditions by King et al.[33] As the creation of a steady-state surface coverage by copper(I) would not be expected to take up to 1.5 days, the activation of the nitrate reaction by soluble copper(I) was the most likely cause of the increase in the rate. The eventual establishment of a steady-state corrosion rate would then have been controlled by the rates of the oxygen and nitrate reduction reactions, with the rate of the latter reaction regulated by the achievement of a steady-state copper(I) concentration. This steady state would be achieved by a balance between the rate of formation of copper(I) as a corrosion product due to oxygen reduction and its rate of consumption by nitrate reduction and by further oxidation to copper(II) by reaction with oxygen as shown in the following equation:

$$4Cu^{+} + O_2 + 4H^{+} \rightarrow 4Cu^{2+} + 2H_2O. \quad (11)$$

Figure 12 shows the steady-state R_p values as a function of the oxygen vol% of the purge gas. A comparison was drawn between these R_p values and those previously collected under aerated, argon-sparged, and anoxic conditions (Figure 3). Under atmospheric conditions, the oxygen vol% was expected to be ~21%,[34,35] suggesting that the final R_p value was between the values collected for 15 and 25 oxygen vol% sparged conditions. The data presented in Figure 12 showed that this was the

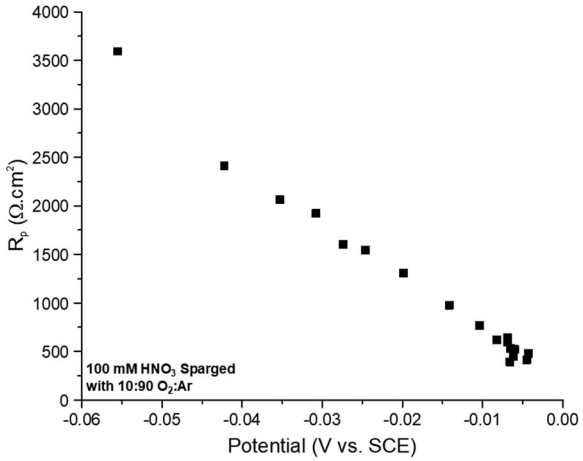

FIGURE 11 E_{corr} versus R_p measurements for 100-mM HNO_3 solutions sparged with 10% O_2 by volume. SCE, saturated calomel electrode

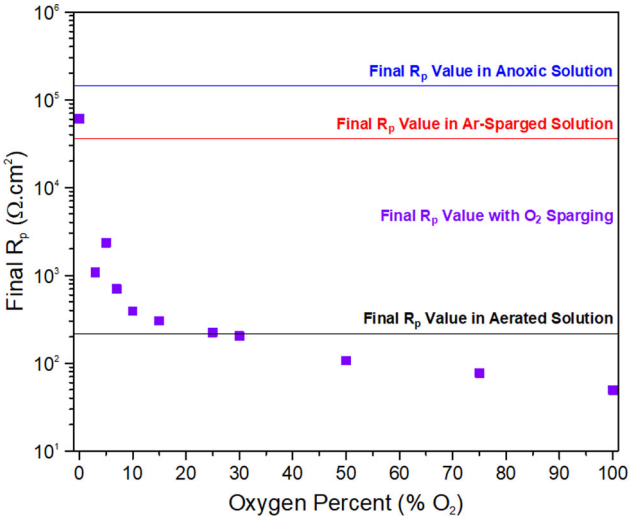

FIGURE 12 Final R_p values recorded as a function of O_2 vol%. Final R_p values from experiments in aerated, Ar-sparged, and anoxic 100-mM HNO_3 are plotted as horizontal lines and used as reference values [Color figure can be viewed at wileyonlinelibrary.com]

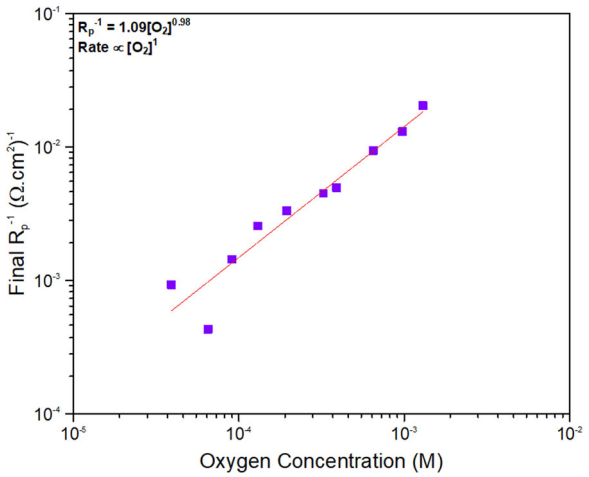

FIGURE 13 The relationship between the pseudo-corrosion rate, R_p^{-1}, and dissolved [O_2] [Color figure can be viewed at wileyonlinelibrary.com]

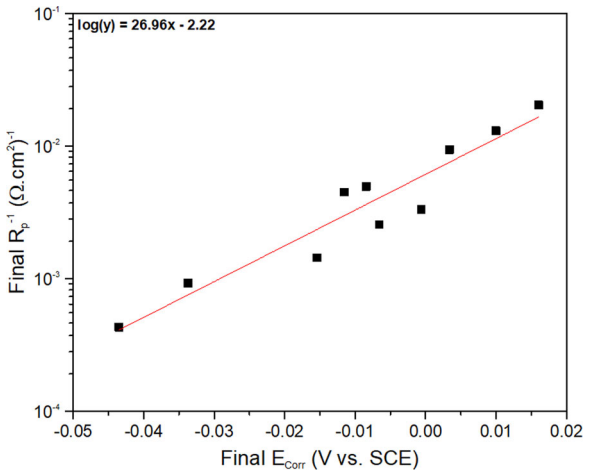

FIGURE 14 The relationship between the pseudo-corrosion rate, R_p^{-1}, and the steady-state E_{corr}. SCE, saturated calomel electrode [Color figure can be viewed at wileyonlinelibrary.com]

case, confirming that rates extracted from this data were in agreement with changing oxygen concentrations under stagnant atmospheric conditions. Figure 13, a plot of log R_p^{-1} versus oxygen concentration, showed that the reaction was first order with respect to oxygen concentration. This would be expected if oxygen was the dominant cathodic reaction since, while the overall four electron transfer reaction,

$$O_2 + 4H^+ + 4e^- \rightarrow 2H_2O, \quad (12)$$

involved multiple reaction steps and would have proceeded through a number of pathways,[36,37] the rate-determining step was the first electron transfer step[33,36–40] with the reaction being first order with respect to oxygen concentration.

Figure 14 shows a plot of log R_p^{-1} versus E_{corr}, which was linear with a slope of 37.1 ± 4.7 mV/decade. As the cathodic reaction was dominant in determining the corrosion kinetics, this slope reflected an extreme dependence, which would be consistent with a catalyzed overall reaction. As the cathodic process involved two reactions, this large dependence reflected the catalytic nature of the overall process, but could not distinguish between contributions from the individual reactions, reactions (7–10) and (12).

Figure 15 shows SEM images of copper surfaces after corrosion in 100-mM nitric acid sparged with argon containing various oxygen contents: 100% oxygen vol%, Figure 15a,b; 50% oxygen vol%, Figure 15c,d; 25% oxygen vol%, Figure 15e,f; and 3% oxygen vol%, Figure 15g,h. As expected from the electrochemical measurements, the degree of corrosion damage decreased with decreasing oxygen vol%. When sparged with 100% oxygen vol%, a significant damage resulted uniformly across the electrode surface. Striations were observed on the electrode surface, with their extent, direction, and frequency and the extent of damage dependent on the crystallographic orientation of the corroded grain. As the oxygen concentration was decreased, the extent of preferential etching decreased, with the grain boundaries becoming more visible, owing to the better defined differences in corrosion morphology on different grains. For the electrode corroded in the solution containing 25% oxygen vol%, the extent of corrosion damage was significantly reduced with some grains sustaining only minimal corrosion. After exposure at 3% oxygen vol%, the corrosion damage was generally distributed across the entire electrode surface. Although roughening of the surface was observed, the original grinding lines were still visible, Figure 15g.

Variations in the distribution of corrosion damage were attributed to the strong adsorption energy of nitrate on copper. Bae et al.[27] investigated the adsorption of nitrate on a copper {100} surface, but the corrosion behavior was only briefly examined. Significantly less corrosion damage was observed on the copper {100} surface in comparison to that on the copper {111} or copper {poly} surfaces.[27] Similar effects were observed on cuprite by Hua et al.,[41] with the crystal plane stability following a similar pattern, $\{100\} \gg \{111\} > \{110\}$.[41] The different adsorption energies provide different levels of protection for the various copper grains. At a high oxygen concentration, oxygen was capable of oxidizing the copper surface to produce copper(I), which subsequently activated the nitrate reduction process, as previously discussed in our previous work.[15] The similarity in damage profiles when the oxygen concentration was high

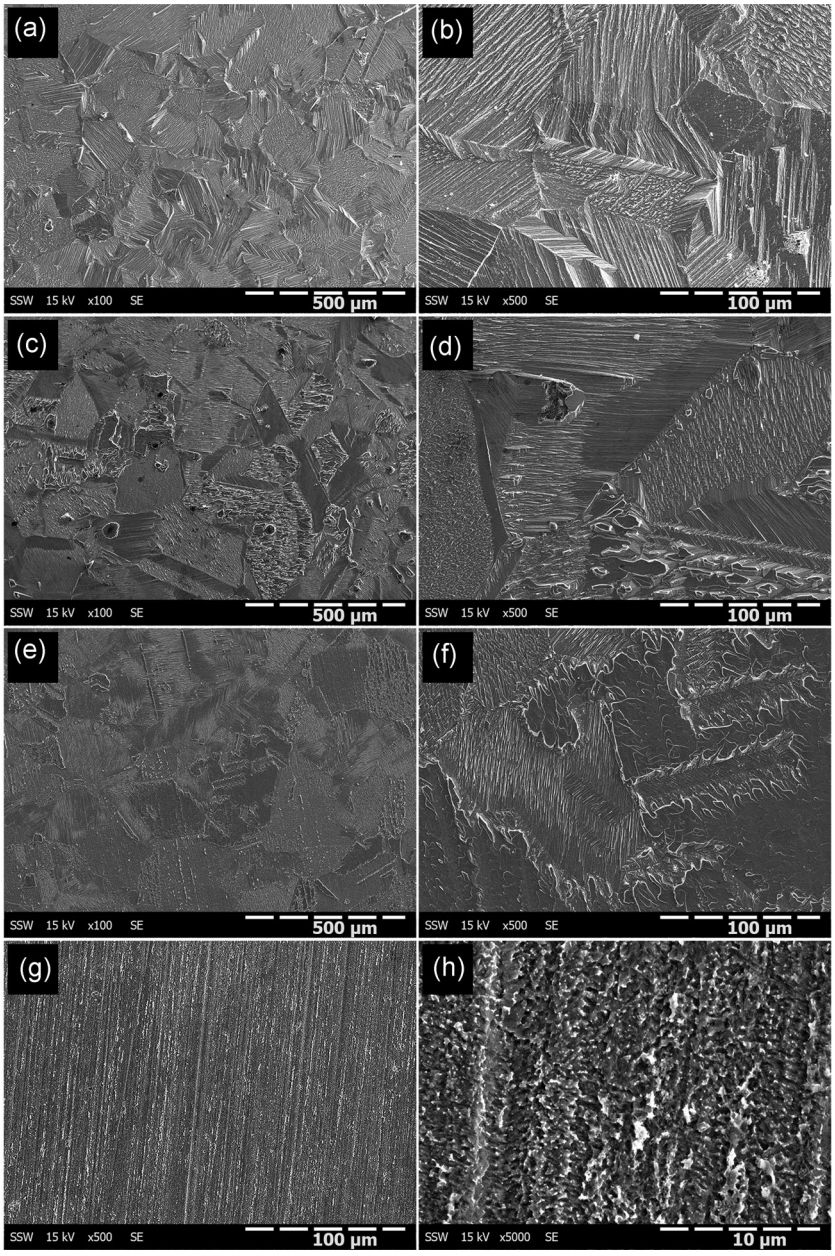

FIGURE 15 Scanning electron micrographs of Cu coupons after 3-day immersion in 100-mM HNO_3 sparged with (a,b) 100% O_2 vol%; (c,d) 50% O_2 vol%; (e,f) 25% O_2 vol%; and (g,h) 3% O_2 vol%

indicated that the differences in nitrate adsorption energy with respect to crystallographic orientation had only a minimal effect when a significant copper(I) concentration was available. At intermediate oxygen concentrations, preferential etching dominated the corrosion morphology. This suggested that the adsorption energy of nitrate could have determined which grains were more susceptible to corrosion, before the concentration of Cu^I in solution reached a steady state, followed by the copper (I)-catalyzed nitrate reduction. Based on the adsorption energies reported in the literature,[27,41] copper {100} grains would have undergone the least corrosion, whereas {111} and {110} would have corroded more readily. As the oxygen concentration decreased, oxygen became less able to displace nitrate from surface adsorption sites, thereby preventing the production of the copper(I) required to activate nitrate reduction. Under these conditions, nitrate partially protected the copper surface, leading to a loss of preferential grain etching and a more general distribution of corrosion damage.

4 | SUMMARY AND CONCLUSIONS

Figure 16 attempts to summarize the influence of dissolved oxygen on the overall corrosion process.

- In the absence of oxygen, corrosion was blocked by the chemisorption of nitrate ($NO_3^-{}_{(ads)}$) on the copper

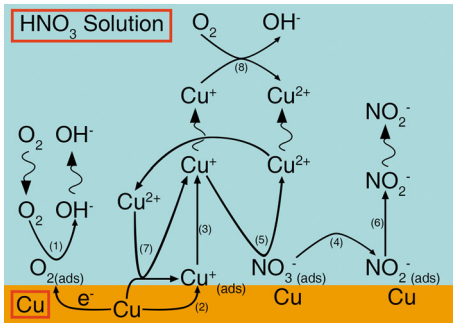

FIGURE 16 A schematic illustrating the mechanistic processes determined to occur on Cu in HNO_3 [Color figure can be viewed at wileyonlinelibrary.com]

surface; however, it was possible that this led to the oxidation of the copper surface to cuprite.

- When oxygen was present, it could compete with nitrate for surface adsorption sites (Process 1).
- Subsequently, $O_{2(ads)}$ oxidized the surface to $Cu^{+}_{(ads)}$ (Process 2), which either acted as a catalyst to accelerate oxygen reduction (not shown) or was released to the acidic solution as copper(I) (Process 3). Further oxidation of $Cu^{+}_{(ads)}$ and release as copper(II) were also possible (not shown).
- Copper(I) then reduced $NO_3^{-}{}_{(ads)}$ to $NO_2^{-}{}_{(ads)}$ (Process 4) while being oxidized to copper(II) (Process 5), with nitrite being released to the solution (Process 6) and diffusing away from the copper surface.
- It was possible that nitrite also acted as an oxidant to enhance copper corrosion, but this study has not investigated that possibility.
- It was also possible that $Cu^{+}_{(ads)}$ could have reduced $NO_3^{-}{}_{(ads)}$, but available literature offers a convincing argument that soluble copper(I) is the reductant.
- The formation of copper(II) in close proximity to the copper surface then initiated the catalytic cycle by further oxidizing copper to copper(I) (Process 7).
- This catalytic cycle could have been promoted by the homogeneous formation of copper(II) by the reaction of copper(I) with oxygen (Process 8).

ACKNOWLEDGMENTS

The authors would like to acknowledge the Nuclear Waste Management Organization and Natural Sciences and Engineering Research Council (NSERC) for the funding used to conduct the research presented in this manuscript. They would also like to acknowledge Surface Science Western for the use of their instruments.

ORCID

Joseph Turnbull http://orcid.org/0000-0002-9717-3308

REFERENCES

[1] T. Standish, J. Chen, R. Jacklin, P. Jakupi, S. Ramamurthy, D. Zagidulin, P. Keech, D. Shoesmith, *Electrochim. Acta* **2016**, *211*, 331.
[2] T. Standish, D. Zagidulin, S. Ramamurthy, P. Keech, J. Noël, D. Shoesmith, *Corros. Eng. Sci. Technol.* **2017**, *52*, 65.
[3] P. Keech, P. Vo, S. Ramamurthy, J. Chen, R. Jacklin, D. Shoesmith, *Corros. Eng. Sci. Technol.* **2014**, *49*, 425.
[4] P. Jakupi, P. Keech, I. Barker, S. Ramamurthy, R. Jacklin, D. Shoesmith, D. Moser, *J. Nucl. Mater.* **2015**, *466*, 1.
[5] C. Boyle, S. Meguid, *Nucl. Eng. Des.* **2015**, *293*, 403.
[6] D. Hall, P. Keech, *Corros. Eng. Sci. Technol.* **2017**, *52*, 2.
[7] F. King, M. Kolar, S. Stroes-Gascoyne, P. Maak, MRS Proceedings **2003**, *807*, 811.
[8] P. Maak, F. King, MRS Proceedings **2006**, *932*, 29.1.
[9] F. King, C. Lilja, M. Vähänen, *J. Nucl. Mater.* **2013**, *438*, 228.
[10] F. King, M. Kolar, P. Maak, *J. Nucl. Mater.* **2008**, *379*, 133.
[11] S. Briggs, J. McKelvie, P. Keech, B. Sleep, M. Krol, *Corros. Eng. Sci. Technol.* **2017**, *52*, 200.
[12] P. Yakabuskie, J. Joseph, J. Wren, *Radiat. Phys. Chem.* **2010**, *79*, 777.
[13] P. Yakabuskie, J. Joseph, C. Stuart, J. Wren, *J. Phys. Chem. A* **2011**, *115*, 4270.
[14] R. Morco, J. Joseph, D. Hall, C. Medri, D. Shoesmith, J. Wren, *Corros. Eng. Sci. Technol.* **2017**, *52*, 141.
[15] J. Turnbull, R. Szukalo, M. Behazin, D. Hall, D. Zagidulin, S. Ramamurthy, J. Wren, D. Shoesmith, *Corrosion* **2017**, *74*, 326.
[16] B. Ibrahim, D. Zagidulin, M. Behazin, J. Wren, D. Shoesmith, *Corros. Sci.* **2018**, *141*, 53.
[17] Å. Bjorkbacka, C. Johnson, C. Leygraf, M. Jonsson, *J. Electrochem. Soc.* **2017**, *164*, C201.
[18] E. Filimonov, A. Shcherbakov, *Prot. Met.* **2004**, *40*, 280.
[19] J. Davis, M. Moorcroft, S. Wilkins, R. Compton, M. Cardosi, *Analyst* **2000**, *125*, 737.
[20] R. Sander, *Atmos. Chem. Phys.* **2015**, *15*, 4399.
[21] C. Zoski, *Handbook of Electrochemistry*, Elsevier, New Mexico **2006**.
[22] M. Biesinger, *Surf. Interface Anal.* **2017**, *49*, 1325.
[23] M. Goldman, C. Tully, J. Noel, D. Shoesmith, *Corros. Sci.* **2020**, *169*, 108607.
[24] R. Partovi-Nia, S. Ramamurthy, D. Zagidulin, J. Chen, R. Jacklin, P. Keech, D. Shoesmith, *Corrosion* **2015**, *71*, 1237.
[25] G. Dima, A. De Vooys, M. Koper, *J. Electroanal. Chem.* **2003**, *554*, 15.
[26] K. Khaled, *Corros. Sci.* **2010**, *52*, 3225.
[27] S. Bae, K. Stewart, A. Gewirth, *J. Am. Chem. Soc.* **2007**, *129*, 10171.
[28] S. Bae, A. Gewirth, *Faraday Discuss.* **2009**, *140*, 113.
[29] M. Biesinger, B. Hart, R. Polack, B. Kobe, R. Smart, *Miner. Eng.* **2007**, *20*, 152.
[30] M. Biesinger, B. Payne, A. Grosvenor, L. Lau, A. Gerson, R. Smart, *Appl. Surf. Sci.* **2011**, *257*, 2717.
[31] F. King, C. Lilja, K. Pedersen, P. Pitkänen, M. Vähänen, *Technical Report SKB-TR-10-67*, Svensk Kärnbränslehantering AB, Solna, Sweden **2010**.
[32] C. Yoder, E. Bushong, X. Liu, V. Weidner, P. McWilliams, K. Martin, J. Lorgunpai, J. Haller, R. Schaeffer, *Mineral. Mag.* **2010**, *74*, 433.

[33] F. King, M. Quinn, C. Litke, *J. Electroanal. Chem.* **1995**, *385*, 45.
[34] N. Giroud, Y. Tomonaga, P. Wersin, S. Briggs, F. King, T. Vogt, N. Diomidis, *Appl. Geochem.* **2018**, *97*, 270.
[35] Y. Tomonaga, N. Giroud, M. Brennwald, E. Horstmann, N. Diomidis, R. Kipfer, P. Wersin, *Appl. Geochem.* **2019**, *100*, 234.
[36] M. Shao, Q. Chang, J. Dodelet, R. Chenitz, *Chem. Rev.* **2016**, *116*, 3594.
[37] Y. Li, Q. Li, H. Wang, L. Zhang, D. Wilkinson, J. Zhang, *Electrochem. Energ. Rev.* **2019**, *2*, 518.
[38] O. Antoine, Y. Bultel, R. Durand, *J. Electroanal. Chem.* **2001**, *499*, 85.
[39] R. Zurilla, R. Sen, E. Yeager, *J. Electrochem. Soc.* **1978**, *125*, 1103.
[40] T. Jiang, G. Brisard, *Electrochim. Acta* **2007**, *52*, 4487.
[41] Q. Hua, D. Shang, W. Zhang, K. Chen, S. Chang, Y. Ma, Z. Jiang, J. Yang, W. Huang, *Langmuir* **2010**, *27*, 665.

How to cite this article: Turnbull J, Szukalo R, Zagidulin D, Biesinger M, Shoesmith D. The kinetics of copper corrosion in nitric acid. *Materials and Corrosion*. 2021;72:348–360.
https://doi.org/10.1002/maco.202011707